# Temporal Evolution of flow in Pore-Networks: From Homogenization to Instability

Ahmad Zareei,* Deng Pan,* and Ariel Amir†
*School of Engineering and Applied Sciences, Harvard University, Cambridge, MA, 02148*
(Dated: May 5, 2021)

We study the dynamics of flow-networks in porous media using a pore-network model. First, we consider a class of erosion dynamics assuming a constitutive law depending on flow rate, local velocities, or shear stress at the walls. We show that depending on the erosion law, the flow may become uniform and homogenize, stay as it is, or become unstable and develop channels. By defining an order parameter capturing different behaviors we show that a phase transition occurs depending on the erosion dynamics. Using a simple model, we identify quantitative criteria to distinguish these regimes that correctly predicts the fate of the network given an erosion dynamics. Lastly, we show that the initial stages of pores clogging show analogous behaviors which depends on the clogging dynamics.

Fluid flow through a porous medium undergoing a dynamical change in its network of micro-structure is a challenging problem and has many environmental and industrial applications[1–14]. The disordered pore structure of a porous medium results in a heterogeneously distributed fluid flow between the pores. Due to the fluid flow, the pore structure can further change dynamically either through the erosion of pore boundary walls or deposition/sedimentation of material on the boundary of the pores. Such heterogeneous and dynamical changes of the solid structure affect the pore-level fluid flow which in turn affects the dynamical changes to the pore structure. This feedback mechanism along with the initial heterogeneous fluid flow complicates the dynamical process and makes it difficult to understand and predict the porous media behavior. Nonetheless, an understanding of the dynamical change is essential to improve any of the porous media applications where the pore network changes over time, applications such as groundwater remediation and precipitation of minerals in rocks[15], biofilm growth in water filtration, and protective filters[4–8], as well as enhanced oil recovery with polymer flooding[16,17], or water-driven erosion[18,19].

In light of the plethora of applications, it is surprising that the evolution of porous structures exposed to erosion and deposition has only been partially understood both theoretically and experimentally. In order to model erosion in porous materials, different models have been used where erosion is assumed to be locally proportional to different flow parameters. Some studies have focused on the erosion of the pore structure proportional to the shear stress at the walls[20–23], or proportional to the power dissipated by the flow[24–26]. More recently it has been shown that using a coarse-grained model with an erosion rate depending on the local pressure gradient, different branching instability can be reached in a porous material[19,27]. Similarly, in clogging, various deposition rates either depending on local fluid flux, velocity, or at a constant rate independent of any flow parameters have been used[28–30]. In order to unify the different approaches, we use a general continuous model which allows us to study the effect of different erosion or clogging dynamics with a single constitutive law. Additionally, we use a network approach[31–35] to study the flow dynamics in the porous media. The network approach has the advantage of not requiring coarse-grained homogenization and is computationally simple allowing us to simulate larger domains.

The network of pores inside the solid structure is connected together through pore-throats that effectively show resistance to the fluid flow between the pores (Fig. 1a). Network-based models have successfully shown to capture key properties of fluid flow in a porous material such as the probability distribution of fluid flux[31], the permeability scaling during clogging[36], or the first fluidized path in a porous structure[37]. The degradation of the solid skeleton (i.e., erosion) or deposition of material on the pore throats (i.e., clogging) in such networks is modeled by the change (increase or decrease) in the radius of the edges connecting the pores which ultimately translates in the changes in the flow resistance between the pores. Using a general local erosion law that can model different dynamics, we show a variety of behaviors are possible. Using numerical simulations with an erosion model on a random network we show the emergence of two behaviors and morphologies (i.e., channelization instability or homogenization) are possible through selective erosion and subsequent flow enhancement. We develop a simplified model to capture the underlying physics and furthermore show a phase transition occurs depending on the parameters of the model.

*Methods and Results*– We consider low-Reynolds fluid flow through the porous network, i.e., $\rho u r/\mu \ll 1$ where $\rho$ is the fluid density and $\mu$ is the kinematic viscosity, $u$ and $r$ are characteristic fluid velocity and pore radius. In such conditions, the fluid flow in each tube follows the Poiseuille law $p_i - p_j = (8\mu l_{ij}/\pi r_{ij}^4) q_{ij}$ where $p_i, p_j$ represent pressures at neighboring nodes $i$, $j$, and $r_{ij}, l_{ij}, q_{ij}$ are respectively the radius, length, and fluid flow rate at the edge connecting pores $i$ and $j$. The coefficient $\pi r_{ij}^4/8\mu l_{ij}$ which relates the fluid flux to the pressure difference can be considered as the conductance $C_{ij}$ of the edge $ij$ in the pore-network. Solving for the conservation of the mass at all pores (inset in Fig. 1b), the pressure distribution over the nodes can be obtained

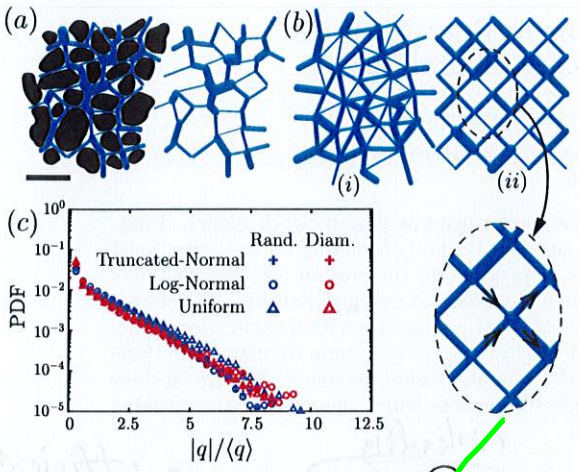


FIG. 1. (a) Cross section of a porous media obtained using computerized tomography (CT) scan of a sandstone sample (CT image taken from[38]). The scale in the bottom left shows 1mm. The network of pores and throats is highlighted in blue. In the network model, the pores are represented with nodes and the throats between pores are approximated with tubes connecting the pores together. (b) Schematic of a topologically random network (i); and a structured diamond grid network (ii). The edge diameters in both networks are randomly distributed. The inset figure shows the conservation of mass at each node. (c) The universal probability distribution function (PDF) of fluid flux for a topologically random (in blue) or diamond network (red) with a highly disordered random net including uniform (triangles), log-normal (circles), and truncated normal (plus) distributions.

(see supplementary material section S1). Initially, we consider a topologically random network of nodes constructed using a uniform distribution of $N_x \times N_y$ nodes in a planar domain where the nodes' connectivity are obtained using Delaunay triangulation (see Fig. 1b(i) for a part of such network). The radius of the edges is considered as independent and identically distributed random variables sampled from a probability distribution that can be either uniform, log-normal, or a truncated normal distribution (see supplementary material S1 for more details). Assuming a pressure difference between the boundary nodes at the left and the right boundary, the pressure at the nodes and the fluid flow rate at the tubes can be obtained by solving the corresponding set of linear equations. We find that for large enough randomness in the edge radii (i.e., $\mathrm{std}(r_{ij})/\mathrm{mean}(r_{ij}) \geq 0.5$), the PDF is well described by a single exponential distribution as shown in Fig. 1c. The exponential form of the PDF reflects the relatively small number of edges with extremely large fluid fluxes. The exponential distribution of fluid flux obtained here is similar to the earlier experimental and numerical measurements[31,36,39]. Considering a structured diamond-grid of pores (Fig. 1b(ii)) which significantly simplifies the geometrical complexity of the network, we find that the PDF of normalized fluid flux remains unchanged for various distributions 1c). The diamond grid allows us to calculate the mean-field approximation of fluid flux distribution (see supplementary material S3) using similar idea proposed for the force distribution in granular materials[31,40,41]. Particularly, it can be shown that the PDF of normalized fluid flux inside a highly disordered porous material converges to a universal distribution with an exponential form, i.e., $p(\hat{q}) \propto e^{-\alpha \hat{q}}$ for large $\hat{q}$ where $\hat{q}$ is the normalized fluid flux $\hat{q} = q/\langle q \rangle$ (see supplementary materials S3). This result indicates a simple method to capture the statistics of heterogeneous fluid flow inside a porous material

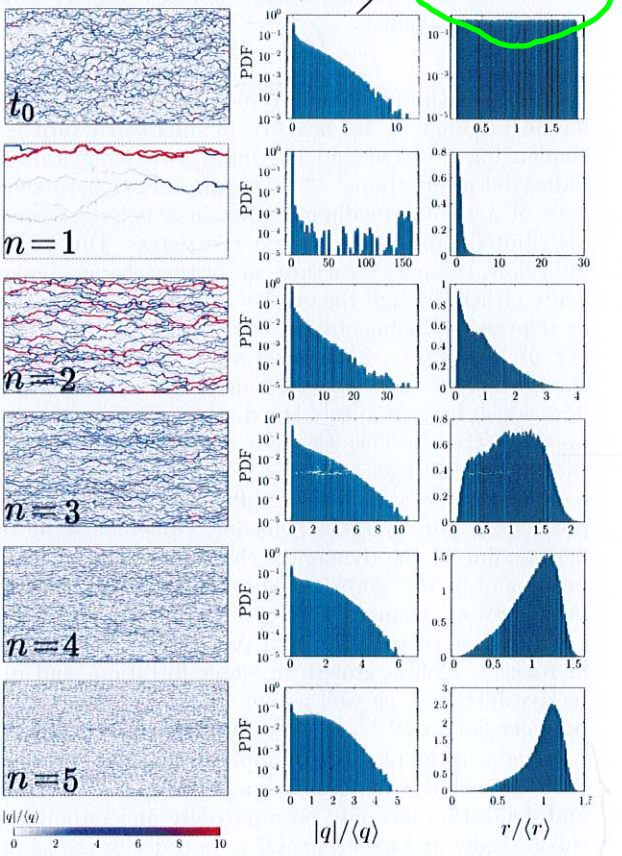


FIG. 2. Erosion in a network of pipes. The initial condition is shown with the label $t = 0$ in the first row. Each row afterward corresponds to the simulation result after $N$ steps such that $\langle r_{t=N} \rangle = 2r_0$ where $r_0 = \langle r_{t=0} \rangle$. The erosion law is based on Eq. (1) where different powers of $n$ correspond to different models of erosion. The first column is a snapshot of the pore network, the second column is the PDF of normalized fluid flux $q/\langle q \rangle$, and the last column is the PDF of normalized radius $r/\langle r \rangle$.

In order to model erosion in porous media, we consider the abrasion in the throats which correspond to the change in the radius of the edges in the network. We

model the dynamics of the change in the radius as

$$\frac{dr_{ij}}{dt} = \alpha \frac{|q_{ij}|^m}{r_{ij}^n} \tag{1}$$

where $m, n, \alpha$ are constants. Different powers of $m$ and $n$ along with a positive $\alpha > 0$ correspond to different physics in the erosion. Particularly, the erosion when $m = 1$ and (i) $n = 0$ depends on the amount of flux $q_{ij}$ passing through the edge; (ii) $n = 2$ depends on the local velocities; (iii) $n = 3$ depends on the shear force at the boundary of the throat. Additionally, $m = 2$ and $n = 6$ corresponds to the models considered in biological transport networks where the radius change has a quadratic dependence on wall shear stress[42,43]. We consider a randomly initialized network with a highly disordered diameters obtained from a uniform distribution (See supplementary material S1). The flow inside the pores, PDF of flux in the tubes, and PDF of tube radii are shown in Fig. 2. We assume a constant pressure difference between the left and the right boundaries. In each time step, we increase the local radius of the tubes based on the erosion law introduced in Eq. (1) with $m = 1$. Since different physics of erosion requires linear dependence of erosion to the flow parameters (such as fluid flux, velocity, or shear stress at the walls, we chose $m = 1$. Later we will address the network's behavior for different powers of $m$. We continue the simulations until $\langle r \rangle = 2r_0$. The results of the simulations for different $n$ are shown in Fig. 2. When $n = 1$ or 2, the network develops channels. In such cases, the flow is dominated by a few edges carrying most of the flow while the rest of the network carries almost no flow. This can be seen in the PDF of the normalized radius which becomes bimodal. Furthermore, the PDF of the normalized fluid flux contains a small number of edges with very large flux values while the majority of the edges carry small flux. Contrary to $n = 1, 2$, when $n = 3$ and the erosion depends on shear at the throats' boundary walls, we find that the flow patterns stay very close to the initial shape, however, with larger and exacerbated flux values. Although the maximum fluid flux increases, the PDF of normalized fluid fluxes remains almost exponential, and the PDF of diameters moves toward larger values. Increasing $n$ to larger values, $n = 4$ or 5, we find that the flow pattern in the network moves toward homogenization. Here, the tail of the normalized fluid flux distribution retracts and the distribution moves toward the average value. We further find that the PDF of the diameters moves toward the average and the coefficient of variation reduces.

*Simplified Model*– In order to understand the underlying reason behind the transition in network behavior during erosion for different powers of $n$, we focus on a simplified model with only two tubes in parallel or series (see Fig. 3a,b). First, assuming two cylindrical tubes with radii $r_1, r_2$ in series and connected back to back, the flow is the same for the two tubes $q_1 = q_2 = q$ (Fig. 3a). The radius of each tube then changes with $dr_i/dt = \alpha q / r_i^n$ where $i = 1, 2$. As a result, we find that the conductivity of each tube changes as $dC_i/dt \propto C_i^{(n-3)/4}$, where each tube's conductivity increases with a rate depending on $n$ (i.e., the larger the $n$ the faster it moves toward

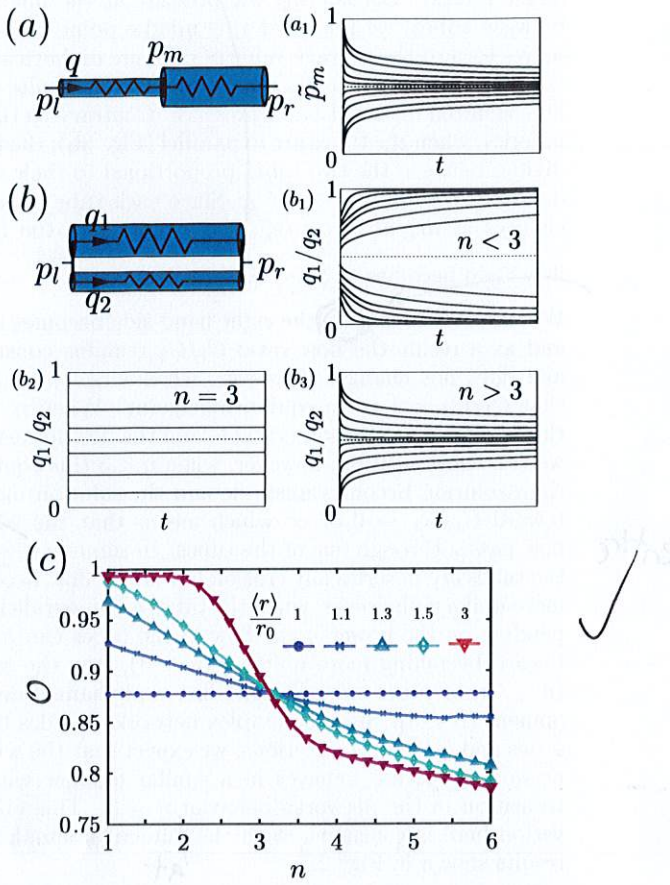


FIG. 3. Two tubes in (a) series or (b) parallel configuration. The tube radius dynamically change with the erosion law (Eq. (1)) with $m = 1$. When the tubes are in series, we find that for any $n$, ($a_2$) the normalized pressure at the middle junction between the tubes $\tilde{p}_m = (p_m - p_l)/(p_r - p_l)$ approaches 1/2 which results in a homogenized pressure distribution. When the tubes are in parallel, initially the flow is distributed among the tubes proportional to their flow conductivity $C_1, C_2$. After erosion, we find that ($b_1$) when $n < 3$, the whole flow eventually passes through one of the tubes, and channeling occurs; ($b_2$) when $n = 3$, the flow ratio between the pipes does not change over time; and ($b_3$) when $n > 3$ the flow distributes between the tubes equally and $q_1/q_2 \to 1$ which results in the homogenization of the network. (c) Order parameter $\mathcal{O}$ calculated from simulation results presented in Fig. 2 for different powers of $n$ plotted over time as the network structure is eroded. In a random network, when $n < 3$ the order parameter increases ($\mathcal{O} \to 1$) while the network is developing channels, and when $n > 3$ the order parameter decreases ($\mathcal{O} \to 0$) while the network moves toward homogenization, and when $n \approx 3$ the order parameter stays constant while the network statistics remains unchanged.

larger values). Considering the pressure at the junction between tubes, we find that this middle point pressure moves toward the average value of pressure on both sides (see Fig. 3($a_1$)) and consequently the erosion results in a homogenized distribution of pressure. Contrary to tubes in series, when the tubes are in parallel (Fig. 3b), the flow divides between the two tubes proportional to their conductivity i.e. $q_1/q_2 = C_1/C_2$. Since each tube's radius changes as $dr_i/dt = \alpha q_i/r_i^n$, the evolution of the fluid flow ratio becomes $\frac{d}{dt}\left(\frac{C_1}{C_2}\right) \propto \frac{C_1}{C_2^{(n+1)/4}}\left(\left(\frac{C_1}{C_2}\right)^{\frac{n-3}{4}} - 1\right)$. When $n = 3$ in Eq. (), the right-hand-side becomes zero and as a result the flow ratio $C_1/C_2$ remains constant and does not change. However, when $n \neq 3$, we find that $C_1/C_2 = 1$ is an equilibrium point. When $n > 3$ this equilibrium solution is stable and the flow moves toward homogenization; however, when $n < 3$ this equilibrium solution becomes unstable and the solution moves toward $C_1/C_2 \to 0$ or $\infty$ which means that the whole flow passes through one of the tubes. In summary, when the tubes are in series any erosion law makes flow become more uniform; however, when the tubes are in parallel depending on the power $n$ the flow in the tubes can move toward becoming more uniform ($n > 3$), stay the same ($n = 3$), or move toward instability and channel development ($n < 3$). Since a complex network includes both series and parallel connections, we expect that the whole network structure behaves in a similar manner with a transition in the networks behavior at $n = 3$. This observation here is consistent with the numerical simulation results shown in Fig. 2.

*Phase transition*– In order to quantify the transition of the network between channeling instability and homogenization, we define an order parameter $\mathcal{O} = \frac{1}{N-1}\left(N - \left(\sum_{ij} q_{ij}^2\right)^2 / \sum_{ij} q_{ij}^4\right)$ where $N$ is the number of edges. The order parameter $\mathcal{O} = 0$ when the flux in all the edges become the same $q_{ij} = \bar{q}$. On the other hand, when fluid flux becomes highly localized with only a few edges with non-zero flux, $\mathcal{O} \to 1$. We numerically calculated the order parameter $\mathcal{O}$ for the diamond-grid network during the erosion process. The results are shown in Fig. 3c for different amounts of erosion measured by the increase in the average diameter $\langle r\rangle/r_0$. As shown in Fig. 3c, at $n \approx 3$ the order parameter, remains unchanged; however for $n > 3$ the order parameter moves toward zero, where the flow becomes more uniform, and for $n < 3$ the order parameter goes toward unity, where channels are developed. The transition in the order parameter indicates a phase transition at $n = 3$ in the long-time behavior of the network which is in agreement with the toy model prediction and simulation results in Fig. 2.

So far we mainly focused on an erosion dynamics with $m = 1$ (see Eq. (1)) since it directly corresponds to different physics of erosion in a network, i.e. an erosion rate with a linear dependence to fluid-flux, velocity, shear-rate at the walls, or even at a constant rate. Considering

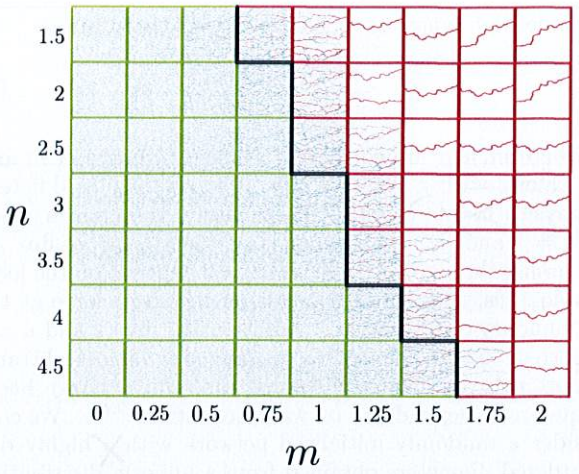


FIG. 4. Evolution of a randomly initialized network for various $m$ . The network is randomly initialized with $N_x = 50$ and $N_y = 50$. The red box and the blue box show the prediction of the simplified model for the fate of network as homogenization (blue) or channelization (red).

$m = 2$ in Eq. (1), our model aligns with the transport optimization problem in biological networks[42–44]. Early works have suggested that in the context of biological transport networks, the network is optimized to minimize its dissipation energy with regards to some constraint (such as constant material/metabolic cost). Interestingly, gradient descent utilized to find the minimal energy configurations maps to Eq. (1) with $m = 2$, albeit with additional regularizing terms. While under the dynamics we study here erosion will occur indefinitely, in biological transport networks a minimal energy configuration exists due to the additional constraints considered in their model. Nonetheless, the minimal energy configurations studied in these biological networks works manifest a phase transition reminiscent of the one we observe in our model. It would be interesting to see if the physical dynamics we have studied here can be mapped to gradient descent on an energy landscape for a general value of $m$. Lastly, to show the effects of a general $m$ in our model, we simulate the general form of erosion dynamics (Eq. (1)). The simulation results for a randomly initialized network for different powers of $m$ and $n$ is shown in Fig. 4, where each box shows the final snapshot of the network eroded with the corresponding $m$ and $n$. We further compare the network's simulation result with the prediction of our simplified model for the fate of the network for each pair of $m, n$. The simplified model's prediction is shown using the bounding box color (red for channelization and green for homogenization) in Fig. 4. Additionally, the solid black line in Fig. 4 shows the simplified model's prediction for the boundary between network's transition to homogeneity or channelization. Although the simplified model is based on the erosion dynamics of two edges in a parallel or series configuration, it still correctly predicts

the fate of the network with the complex connections for different values of $m$ and $n$, and capture the boundary separating channelization/homogenization.

*Conclusion*– In summary, we analyzed the dynamics of the porous networks during erosion. We showed that depending on different erosion laws various network behaviors are observable. Using a simple erosion law, inspired by previously proposed models, we showed that depending on the rate of erosion the network can either move toward homogenization or toward developing a channeling instability. With a simplified model, we elucidated the physical origin of the phase transition. Our results signify the importance of local dynamics and feedback mechanism in long-time global behavior and complement similar feedback-induced studies for active conducting mediums[45].

*Acknowledgments*– We would like to acknowledge Kavli Institute for the fruitful discussions and also MRSEC DMR-2011754 and DMR-1420570 for [illegible] support.

* A.Z. and D.P. contributed equally.
† arielamir@seas.harvard.edu

[1] D. Fraggedakis, C. Kouris, Y. Dimakopoulos, and J. Tsamopoulos, Physics of Fluids **27**, 082102 (2015).
[2] M. Sahimi, *Flow and transport in porous media and fractured rock: from classical methods to modern approaches* (John Wiley & Sons, 2011).
[3] W. H. Schlesinger, Science **284**, 2095 (1999).
[4] J. Herzig, D. Leclerc, and P. L. Goff, Industrial & Engineering Chemistry **62**, 8 (1970).
[5] C. Tien and A. C. Payatakes, AIChE Journal **25**, 737 (1979).
[6] D. P. Jaisi, N. B. Saleh, R. E. Blake, and M. Elimelech, Environmental Science & Technology **42**, 8317 (2008).
[7] M. Carrel, V. L. Morales, M. A. Beltran, N. Derlon, R. Kaufmann, E. Morgenroth, and M. Holzner, Water Research **134**, 280 (2018).
[8] J. D. Seymour, J. P. Gage, S. L. Codd, and R. Gerlach, Physical Review Letters **93**, 198103 (2004).
[9] M. Duduta, B. Ho, V. C. Wood, P. Limthongkul, V. E. Brunini, W. C. Carter, and Y.-M. Chiang, Advanced Energy Materials **1**, 511 (2011).
[10] H. Sun, J. Zhu, D. Baumann, L. Peng, Y. Xu, I. Shakir, Y. Huang, and X. Duan, Nature Reviews Materials **4**, 45 (2019).
[11] S. Marbach, K. Alim, N. Andrew, A. Pringle, and M. P. Brenner, Physical Review Letters **117**, 178103 (2016).
[12] A. Tero, S. Takagi, T. Saigusa, K. Ito, D. P. Bebber, M. D. Fricker, K. Yumiki, R. Kobayashi, and T. Nakagaki, Science **327**, 439 (2010).
[13] K. Alim, G. Amselem, F. Peaudecerf, M. P. Brenner, and A. Pringle, Proceedings of the National Academy of Sciences **110**, 13306 (2013).
[14] L. L. Heaton, E. López, P. K. Maini, M. D. Fricker, and N. S. Jones, Proceedings of the Royal Society B: Biological Sciences **277**, 3265 (2010).
[15] M. N. Rad, N. Shokri, and M. Sahimi, Physical Review E **88**, 032404 (2013).
[16] L. W. Lake, R. Johns, B. Rossen, G. A. Pope, *et al.*, *Fundamentals of Enhanced Oil Recovery*, (2014).
[17] S. Parsa, E. Santanach-Carreras, L. Xiao, and D. A. Weitz, Physical Review Fluids **5**, 022001 (2020).
[18] N. Schorghofer, B. Jensen, A. Kudrolli, and D. H. Rothman, Journal of Fluid Mechanics **503**, 357 (2004).
[19] A. Mahadevan, A. Orpe, A. Kudrolli, and L. Mahadevan, Europhysics Letters **98**, 58003 (2012).
[20] R. Jäger, M. Mendoza, and H. J. Herrmann, Physical Review E **95**, 013110 (2017).
[21] L. Ristroph, M. N. Moore, S. Childress, M. J. Shelley, and J. Zhang, Proceedings of the National Academy of Sciences **109**, 19606 (2012).
[22] W. Hacking, E. VanBavel, and J. Spaan, American Journal of Physiology-Heart and Circulatory Physiology **270**, H364 (1996).
[23] C. F. Wan and R. Fell, Journal of Geotechnical and Geoenvironmental Engineering **130**, 373 (2004).
[24] H. Steeb, S. Diebels, and I. Vardoulakis, "Modeling internal erosion in porous media," in *Computer Applications In Geotechnical Engineering*, pp. 1–10.
[25] D. Marot, V. D. Le, J. Garnier, L. Thorel, and P. Audrain, European Journal of Environmental and Civil Engineering **16**, 1 (2012).
[26] L. Sibille, F. Lominé, P. Poullain, Y. Sail, and D. Marot, Hydrological Processes **29**, 2149 (2015).
[27] N. J. Derr, D. C. Fronk, C. A. Weber, A. Mahadevan, C. H. Rycroft, and L. Mahadevan, Physical Review Letters **125**, 158002 (2020).
[28] H. Yang and M. T. Balhoff, AIChE Journal **63**, 3118 (2017).
[29] L. N. Reddi, X. Ming, M. G. Hajra, and I. M. Lee, Journal of Geotechnical and Geoenvironmental Engineering **126**, 236 (2000).
[30] G. Boccardo, D. L. Marchisio, and R. Sethi, Journal of Colloid and Interface Science **417**, 227 (2014).
[31] K. Alim, S. Parsa, D. A. Weitz, and M. P. Brenner, Physical Review Letters **119**, 144501 (2017).
[32] I. Fatt *et al.*, Transactions of the AIME **207**, 144 (1956).
[33] M. J. Blunt, B. Bijeljic, H. Dong, O. Gharbi, S. Iglauer, P. Mostaghimi, A. Paluszny, and C. Pentland, Advances in Water resources **51**, 197 (2013).
[34] N. Stoop, N. Waisbord, V. Kantsler, V. Heinonen, J. S. Guasto, and J. Dunkel, Journal of Non-Newtonian Fluid Mechanics **268**, 66 (2019).
[35] S. L. Bryant, P. R. King, and D. W. Mellor, Transport in porous media **11**, 53 (1993).
[36] S. Parsa, A. Zareei, E. Santanach-Carreras, E. Morris, A. Amir, L. Xiao, and D. A. Weitz, arXiv (2021).
[37] D. Fraggedakis, E. Chaparian, and O. Tammisola, Journal of Fluid Mechanics **911**, A58 (2021).
[38] L. T. Akanji and S. K. Matthai, Transport in Porous Media **81**, 241 (2010).
[39] S. S. Datta, H. Chiang, T. Ramakrishnan, and D. A. Weitz, Physical Review Letters **111**, 064501 (2013).
[40] C.-h. Liu, S. R. Nagel, D. Schecter, S. Coppersmith, S. Majumdar, O. Narayan, and T. Witten, Science **269**, 513 (1995).
[41] S. Coppersmith, C.-h. Liu, S. Majumdar, O. Narayan, and T. Witten, Physical Review E **53**, 4673 (1996).

[42] D. Hu and D. Cai, Physical Review Letters **111**, 138701 (2013).
[43] H. Ronellenfitsch and E. Katifori, Physical Review Letters **117**, 138301 (2016).
[44] F. Corson, Physical Review Letters **104**, 048703 (2010).
[45] S. A. Ocko and L. Mahadevan, Physical Review Letters **114**, 134501 (2015).